INSTITUTE OF PHYSICS PUBLISHING JOURNAL OF PHYSICS: CONDENSED MATTER

J. Phys.: Condens. Matter **16** (2004) S2629–S2642 PII: S0953-8984(04)72912-4

Development of an interatomic potential for phosphorus impurities in α-iron

G J Ackland[1], M I Mendelev[2], D J Srolovitz[2], S Han[3] and A V Barashev[4]

[1] School of Physics, The University of Edinburgh, Mayfield Road, Edinburgh EH9 3JZ, UK
[2] Princeton Materials Institute, Princeton University, Princeton, NJ 08544, USA
[3] Department of Physics, Ewha Womans University, Seoul 120-750, Korea
[4] Department of Engineering, The University of Liverpool, Liverpool L69 3GH, UK

Received 1 December 2003
Published 25 June 2004
Online at stacks.iop.org/JPhysCM/16/S2629
doi:10.1088/0953-8984/16/27/003

Abstract

We present the derivation of an interatomic potential for the iron–phosphorus system based primarily on *ab initio* data. Transferability in this system is extremely problematic, and the potential is intended specifically to address the problem of radiation damage and point defects in iron containing low concentrations of phosphorus atoms. Some preliminary molecular dynamics calculations show that P strongly affects point defect migration.

(Some figures in this article are in colour only in the electronic version)

1. Introduction

Phosphorus is one of the major causes of embrittlement of nuclear reactor pressure vessel (RPV) steels [1]. A huge enhancement of the concentration of phosphorus (P) atoms at grain boundaries is observed in samples of RPV steels taken from nuclear reactors [2]. This leads to a decrease in the grain boundary cohesion and consequently to a shift of the ductile-to-brittle transition temperature.

A theoretical understanding of the problem requires a full understanding of the interaction of millions of these two atoms at the atomic level. First-principles calculations provide the most reliable way to describe interactions, but they are impractical for large scale molecular dynamics. Hence there is a need for accurate descriptions of the energy based on interatomic potentials which do not treat the electrons explicitly.

A crucial aspect of atomic level modelling is proper relaxation of atoms around the defect, for which elegant methods were developed by Norgett [3]. With state-of-the-art *ab initio* methods it is now possible to treat a few hundred movable atoms: just as with empirical potentials in the seventies this brings problems of finite size effects to the fore and many of the concepts pioneered by Norgett and encapsulated in his DEVIL [4] (defect evaluation in lattices) code are being revisited today, and indeed many of the applications such as dislocation core structure [5] and twin boundaries [6] are still debated.

Here we present the derivation of an interatomic potential for Fe–P which can be evaluated as quickly as a short ranged pairwise potential. For molecular dynamics purposes in studying reactor steels, the interesting region is that of small concentrations ($\sim 10^{-3}$) of P in Fe, in particular, the behaviour of point defects in lattices. Traditionally, data for fitting potentials came from experiment, typically bulk properties, but recently *ab initio* total energy calculation enables us to add more specific atomistic level configurations to the fitting data set. Here we incorporate both *ab initio* and experimental data to parametrize a potential for the dilute P–Fe system.

We choose to write the potential in the form

$$U = \sum_i F_i \left[\sum_j \phi(r_{ij}) \right] + \sum_{ij} V(r_{ij}). \tag{1}$$

For $F_i[x] = \sqrt{x}$ this is the second-moment tight binding form of Cyrot [7] and Finnis and Sinclair [8]. This is transferable between environments where the local band structure is primarily changed by scaling [9]. We will need to fit seven functions for the two-component system: three pair potentials, $V_{\mathrm{FeFe}}(r)$, $V_{\mathrm{FeP}}(r)$ and $V_{\mathrm{PP}}(r)$, three pairwise functions, $\phi_{\mathrm{FeFe}}(r)$, $\phi_{\mathrm{FeP}}(r)$ and $\phi_{\mathrm{PP}}(r)$, and two embedding energy functions, F_{Fe} and F_{P}.

A previous parametrization in this form for general properties of iron [10] gave good qualitative results but was not tailored specifically to defect properties. Recent *ab initio* work [12, 13] shows that at high densities the resistance to compression arises from a many-body effect (electronic kinetic energy) rather than a pairwise repulsion. Fitting compression data using the short range part of $V(r_{ij})$ typically leads to an overestimate of interstitial formation energies and volumes [14]. These quantities have recently come into the realm of what can be calculated by *ab initio* means, and can be used to fit short range repulsion in regions where the density is close to its bulk value. We have shown that including different things in the fit leads to very different potentials: to describe point defect interactions, one must fit point defect properties and so we use an iron potential optimized for point defects as the basis of the present work [13]. This incorporates the kinetic energy effect by writing $F(x) = -\sqrt{x} + a_2x^2 + a_4x^4$, with increasing x taking us smoothly between hopping and free-electron dominated regimes. Hence isotropic compression is dealt with by the many-body term (high x), while short atom–atom distances can be addressed with the pair potential $V(r_{ij})$. This modest change to the second-moment formalism gives greater fitting flexibility and no additional computing cost, since F is implemented via a look-up table.

Pure P is covalently bonded and cannot be described by this type of potential. We therefore do not attempt to fit properties of pure phosphorus, or phosphorus-rich compounds, concentrating instead on point defects in α-iron, their interactions with phosphorus atoms and fictitious iron-rich compounds. To parametrize the potential we use data generated from *ab initio* plane wave pseudopotential calculations using density functional theory [16], ultrasoft pseudopotentials [17], the spin-dependent generalized gradient approximation for exchange and correlation [18] and periodic boundary conditions. Calculations on pure iron [19] suggest that this is a reliable approach; it has been deployed widely and the calculations can be routinely done using standardized software[5].

There is an additional caveat for ferromagnetic materials: the magnetism (and hence Fermi level) is affected by defects and this leads to a much slower convergence of the energy with system size (and k-point sampling) than is typically observed for non-magnetic elements [20]. This may be due to the fact that the Fermi energy moves relative to the spin bands in the supercell calculation, whereas for a truly infinite crystal the bands are fixed. Despite this

[5] Codes PWSCF (www.pwscf.org) and VASP (cms.mpi.univie.ac.at/vasp).

Table 1. Energies of relaxed iron-rich crystal structures ('stripe' is a layer bcc structure with Fe–Fe–Fe–P (001) layers), single-substitutional-impurity (SSI) phosphorus atoms, near neighbour double-substitutional impurity (DSI) and an (001) monolayer of P in seven layers of Fe (labelled Fe_7P) both under strain and after fracture at the P (Fe_7P), one layer above the P (Fe_6PFe) and in pure iron (Fe_8). Stresses are parallel and perpendicular to the long (z) axis respectively. The quoted energies are relative to a spin-zero GGA representation of an iron atom. Absolute values are not used in the fitting, only differences between them for which this arbitrary zero cancels out.

Formula	Structure	Energy (eV)	Mag. mom.	Volume (Å^3)	Pressure (kbar)
Fe_2	bcc	16.617	4.62	23.24	0
Fe_3P	$L1_2$	30.755	7.85	47.59	0
Fe_3P	DO_3	30.971	5.46	43.55	0
Fe_3P	Stripe	30.786	5.52	44.69	0
Fe_6P_3	Fe_2P	69.718	9.13	101.34	0
$Fe_{15}P$	SSI	130.867	35.30	185.9	1.34
$Fe_{53}P$	SSI	446.714	125.26	630.4	0
$Fe_{14}P_2$	DSI	128.407	32.71	185.9	6.67
Formula	Strain, ϵ_{zz}	Energy (eV)	Mag. mom.	Volume (Å^3)	Stresses
Fe_7P	−0.025	63.997	14.6	88.24	65, 82
Fe_7P	0.0	64.066	14.8	90.51	25, 10
Fe_7P	0.025	64.042	15.0	92.77	−13, −51
Fe_7P	0.050	63.941	15.2	95.03	−45, −98
Fe_7P	0.075	63.789	15.6	97.30	−70, −130
Fe_7P	0.5	61.073	10.9	135.76	−26, 0
Fe_6PFe	0.5	60.988	6.9	135.76	−24, 0
Fe_8	0.5	64.141	21.0	135.76	−6, 0

slow convergence of defect energy, the energy differences between e.g. different interstitial configurations converge much more rapidly [19]. Thus we are justified in fitting energy differences from calculations using relatively small unit cells, while obtaining the absolute formation energy from larger calculations.

Ferromagnetism also means that the band structure changes dramatically at the fcc–bcc phase transition iron. For this reason [9] we do not expect the potential to describe paramagnetic iron correctly: high T fcc–bcc transitions have been observed with other iron potentials but the driving force is vibrational (entropic) not magnetic [15].

2. Methods

The fitting strategy assumes that phosphorus interacts with point defects via short ranged, pairwise interactions and long range strain fields. Thus we include configurations representing point defects, single-substitutional-impurity (SSI) phosphorus atoms and combinations thereof. Since the major problem associated with phosphorus is segregation to grain boundaries, we include Fe with a 2D layer of P in our fitting database. By fitting relaxation volumes, we capture long range strain effects. We also include liquid configurations to ensure that the functions are sampled at all separations [29].

The *ab initio* calculations and configurations included in the fitting are given in tables 1–3. Our *ab initio* calculations use small unit cells, which introduces problems of images and relaxation [4] for considering isolated defects. However, by fitting *the same* small cells described by the potential, we alleviate this problem.

The most crucial aspect for radiation damage is the geometry of the defects and barriers (which governs diffusion mechanisms) and the energy differences between them (which

Table 2. Calculated results for interstitial formation energies, relative to GGA free atoms/pure iron and SSI phosphorus. Fe_{17} denotes iron interstitials, $Fe_{16}P$ denotes mixed dumb-bells or P interstitials, $Fe_{15}P_2$ denotes P–P dumb-bells. TET and OCT denote tetrahedral and octahedral sites respectively; other structures are dumb-bell configurations. In each case the volume is constrained to the 16-atom pure iron cell, a $9 \times 9 \times 9$ k-point grid was used and all atomic positions relaxed. The mixed dumb-bells have low symmetry and may relax to a higher symmetry state: the [001] mixed dumb-bell relaxes to the octahedral position and the [111] mixed dumb-bell goes to the crowdion position. These calculations are for small supercells incorporating both interstitial formation energy and strain interactions—they should not be regarded as energies of isolated defects (they are probably upper bounds). Cohesive energies are quoted firstly relative to non-magnetic free atoms with GGA secondly relative to solid Fe and substitutional $Fe_{15}P$. Comparison with results for larger supercells [19] suggests that full relaxation in a large supercell would lower the formation energies systematically by about 1 eV. Elastic correction for finite size [27] of $P^2V/2B$ suggested that full relaxation in a large supercell would lower the formation energies systematically by about 1.5 eV.

Formula	Structure	Energy (eV)	Strain adjusted	Mag. mom.	Volume (Å^3)	Pressure (kbar)
$Fe_{15}P_2$	111	132.470/4.636	2.91	33.8	185.9	218
$Fe_{15}P_2$	001	132.464/4.642	2.45	33.3	185.9	246
$Fe_{15}P_2$	011	133.419/3.687	1.88	34.1	185.9	223
$Fe_{16}P$	TET	134.828/4.347	2.85	32.8	185.9	203
$Fe_{16}P$	001	134.428/4.747	2.45	35.8	185.9	252
$Fe_{16}P$	011	135.353/3.822	2.39	32.7	185.9	198
$Fe_{16}P$	111	134.820/4.355	2.53	35.7	185.9	224
$Fe_{16}P$	OCT	134.428/4.747	2.44	35.8	185.9	252
Fe_{17}	TET	135.723/5.521	4.29	31.4	185.9	184
Fe_{17}	011	136.419/4.825	2.36	34.2	185.9	201
Fe_{17}	001	134.779/6.466	4.65	34.6	185.9	224
Fe_{17}	111	135.746/5.498	4.03	34.9	185.9	201
Fe_{17}	OCT	134.530/6.715	4.83	35.0	185.9	228

Table 3. Calculated results used to fit vacancy formation energies, relative to GGA free atoms/pure iron and SSI phosphorus. Formulae give the number of atoms in the supercell, 'divac' represents two vacancies at nearest and second-neighbour sites. '1st' and '2nd' represent the site of the P relative to the vacancy, 'bar' represents the energy with the P midway along its migration path. In 15-atom cases, the unit cell and atomic positions are fully relaxed and a $9 \times 9 \times 9$ k-point grid used. These vacancy-rich configurations incorporate both vacancy formation energy and strain interactions—they should not be regarded as energies of isolated defects. In particular, for the second-neighbour cases we have a chain of second-neighbour vacancies. Comparison with results for larger supercells [19] suggests that full relaxation in a large supercell would lower the energies slightly, but maintain the differences between them.

Formula	Structure	Energy (eV)	Mag. mom.	Volume (Å^3)	Pressure (kbar)
Fe_{15}	Vacancy	122.606/2.021	36.4	183.66	0
Fe_{14}	Divac–1st	112.563/3.757	34.9	180.20	0
Fe_{14}	Divac–2nd	112.838/3.481	35.5	179.10	0
$Fe_{14}P$	1st	120.852/1.706	33.2	181.78	0
$Fe_{14}P$	2nd	120.379/2.180	34.6	184.64	0
$Fe_{14}P$	Bar–111	120.504/2.055	33.7	184.14	0
$Fe_{30}P$	1st	253.873/1.622	71.1	371.87	−15
$Fe_{30}P$	2nd	253.775/1.719	72.3	371.87	−7
$Fe_{30}P$	Bar–100	252.006/3.489	70.8	371.87	−19
$Fe_{30}P$	Bar–111	253.525/1.970	71.1	371.87	−8

governs diffusion rates). 'Geometry' here includes the symmetry of the defects and their P composition, but not detailed interatomic separations. Similarly important are the interaction

strengths between phosphorus and point defects, which determine whether pinning of defects occurs. Of secondary importance are the actual values of the formation energies: this affects production rates in cascade simulations, but in a molecular dynamics run defects are very unlikely to be generated thermally.

2.1. Ab initio calculations

Our *ab initio* calculations are done using standard codes (see footnote 5), implementing the pseudopotential plane wave method using density functional theory [16], ultrasoft pseudopotentials [17], the spin-dependent generalized gradient approximation for exchange and correlation [18] and periodic boundary conditions. The plane wave cut-off of 300 eV has been used throughout with k-point convergence to 0.01 eV, force convergence to 0.001 eV Å^{-1} and stress to 0.01 kbar.

Previous *ab initio* calculations on the iron–phosphorus system [21–24] using the similarly reliable full-potential linearized augmented plane wave method have downplayed total energy and concentrated on the role of increased electron density as indicating strengthening of the bonds at the surface relative to the grain boundary. This qualitative picture is not specific to FeP and follows from the tight binding formalism [7]. We observe similar increased electron densities in our calculations of a single layer of P in Fe, but do not use them in fitting.

The actual energies calculated by DFT relative to the free atom are known to be unreliable. Likewise, the Finnis–Sinclair formalism cannot be expected to be transferable to free atoms. Thus we do not at any stage fit the *ab initio* energies directly; rather, we fit relative energies between different configurations of the same number and type of atoms. We take the experimental cohesive energy for α-iron (4.316 eV/atom), but the cohesive energy for phosphorus is not fitted (and nor is the crystal structure of pure phosphorus). All fits are to energy differences with phosphorus in various locations, with the single substitutional impurity taken as the reference state.

2.1.1. Crystal structures (table 1). Several crystal structures were examined and used in the fitting. At the Fe_3P composition we looked at fictitious $L1_2$ (fcc equivalent), DO_3 and DO_{32} (bcc equivalents) and a bcc-based structure with every fourth (001) layer replaced by phosphorus. DO_3 was noticeably lower in energy.

We also calculated Fe_2P, a complex structure which does exist experimentally, finding excellent agreement $a = 5.836$ (experiment: 5.865), $c = 3.436$ (experiment: 3.456), $u = 0.257$ (experiment: 0.256), $v = 0.591$ (experiment: 0.594). This gives us confidence that the *ab initio* calculations are reliable for the system. Results are given in table 1.

2.1.2. Monolayers and surfaces (table 1). To include fracture-relevant data, we evaluated surface energies for pure Fe, Fe with a monolayer of P at the surface, and Fe with a monolayer of P one layer below the surface (there is evidence that P-rich grain boundary fracture occurs by breaking of Fe–Fe bonds adjacent to the boundary, rather than Fe–P bonds at the boundary). The results show that phosphorus does not segregate into a monolayer, either in bulk or on the surface, and that a free (001) surface with P on it has a higher energy than without (taking substitutional phosphorus as the reference state). Assuming replacement of iron by P, the segregation to grain boundaries must result from the different crystalline environment there rather than an intrinsic tendency of P to form layers (by extension, some grain boundaries will be more susceptible than others). Moreover, the fracture embrittlement probably arises from a stress concentration effect rather than a simple Griffith-criterion energy balance. We note however that some experimental evidence [25] suggests that P sits in hollow sites on Fe(001)—

investigating all such possible reconstructions by *ab initio* calculation would be impractical, hence the need for reliable potentials.

2.1.3. Substitutional impurities (table 1). Phosphorus has a small range of solid solubility in Fe, and is believed to be located substitutionally. Several configurations were calculated: a single P atom in a 16(54) ($2^3(3^3)$ bcc) supercell and a pair of P atoms on neighbouring sites in similar cells. In each case all ions were relaxed and we took the calculations to k-point convergence (729/216 k-points). We compared the effects of fixing the lattice parameter at the pure Fe value, or relaxing it to minimize energy (see table 2). The finite size effects going from 16 to 54 atoms were only about 0.1 eV, within the fitting errors. In practice the $Fe_{15}P$ SSI value is used as the P reference state.

The addition of P impurities causes a striking reduction of 10–15% in the stiffness of iron. We calculate elastic constants by applying finite strains and measuring resultant stress. Our calculations for pure iron give elastic constants of $C_{11} = 225$ GPa, $C_{12} = 124$ GPa, $C_{44} = 101$ GPa, some 10% lower than experiment (and therefore not included in the fitting). Calculations on the $Fe_{15}P$ substitutional impurity supercell (6.25% P) give $C_{11} = 196$ GPa, $C_{12} = 109$ GPa, $C_{44} = 91$ GPa.

2.1.4. Vacancies (table 2). With a 31-atom Fe unit cell, we find a vacancy formation energy of 1.94 eV compared to the fully converged value of 1.95 eV [19]. With 30 + 1 atoms, the energy required to create a vacancy adjacent to a substitutional phosphorus is 1.64 eV for the near neighbour site and 1.72 eV for the second-neighbour site.

For 15-atom supercells, the energies are 1.71 eV for the near neighbour site and 2.18 eV for the second-neighbour site; this latter suggests a P–vacancy repulsion, but the cell is so small that the calculation actually represents an alternating chain P–vacancy–P–vacancy, so we neglect it.

We estimate the migration barrier by replacing two atoms in pure Fe with one located at their mid-point[6] and relaxing the remaining atoms while constraining the mirror plane symmetry. As we shall see, in bcc this is not necessarily the barrier for a $(\frac{1}{2}, \frac{1}{2}, \frac{1}{2})$ hop but it does represent a useful configuration to include in the fitting. The energy for P to hop from the near neighbour site into the vacancy is much lower than for the direct second-neighbour [001] hop: in the fitting we ensure that the latter barrier is high enough not to be surmountable in MD.

2.1.5. Interstitials (table 2). In common with experimental [26] and previous work [19, 10] we find the [011] Fe–Fe dumb-bell configuration to be the stable interstitial. Geometrically, the migration mechanism for an [011] interstitial could go via the [111], tetrahedral, octahedral or [001] configuration—our calculations suggest that the tetrahedral and [111] configurations are similar in energy. Dynamically, it is also possible that a process of excitation to (111) followed by fast 1D migration may be favoured [10].

Although we use smaller supercells without relaxation, the difference in energies from larger calculations can be approximated by means of elasticity [27], and the differences between various conformations (which is what we fit) are converged to within the accuracy with which we can fit them. When one or two phosphorus atoms form part of the interstitial the energy is lowered as compared with an iron interstitial and substitutional phosphorus, and the stable configuration remains the [011] dumb-bell.

[6] $(\frac{1}{4}, \frac{1}{4}, \frac{1}{4})$ is the symmetric mid-point; however, if no relaxation occurs the migrating atom makes its closest approach to other neighbours at $(\frac{1}{6}, \frac{1}{6}, \frac{1}{6})$ and $(\frac{1}{3}, \frac{1}{3}, \frac{1}{3})$.

Table 4. Energies and dilatations of defect configurations calculated using the interatomic potential, with 2000-atom constant (zero-) pressure static relaxation. The notation is as for previous tables. 'Energy' refers to a reference state with an equivalent number of iron atoms in pure iron and phosphorus atoms as SSIs in iron. For unstable interstitial configurations we indicate the local minimum. 'Dilatation' is defined relative to pure iron and calculated using constant volume and elastic constants [35].

Structure	Energy (eV)	Dilatation (%)
Pure iron	4.013	0
Fe vacancy	1.71	−22.3
Fe divac-1st	3.285	−35.3
Fe divac-2nd	3.18	−48.9
Bar–Vacancy–Fe	2.34	—
Int 110	3.59	+124.7
Int OCT	4.22	+102.1
Int 100	Int oct	
Int 111	Int 110	
P SSI	0.0	−34.3
P–vac (1st)	1.34	−57.1
P–vac (2nd)	1.37	−58.1
Bar P–vac	1.65	—
P-110	2.57	+115.7
P-111	3.30	+102.7
P-100	Int 110	
P-TET	2.80	+151.5
P-OCT	3.47	+161.5
Bar P-SSI-110	0.27	—

2.1.6. Liquid state calculations. We use a self-consistent process to model liquids, starting with pair potentials [28] and MD to create a 'typical' atomic level model of liquid Fe–P alloy (84 Fe atoms, 12 P). Then the total forces acting on each atom in this model are obtained from static first-principles calculations. We then use dynamical refitting [11] via force matching [31] to produce a new trial potential and generate a new 'typical' liquid configuration with classical MD. The process is then iterated to self-consistency. Liquid configurations provide data across the range of possible Fe–P separations, including small separations which are absent in equilibrium crystal data at $T = 0$, and ensure there are no anomalous wiggles in the potential at separations for which there are no data.

2.2. Fitting

In addition to the *ab initio* calculations above, other properties of pure iron fitted to experiment are $C_{11} = 1.517\,\text{eV Å}^{-3}$, $C_{12} = 0.861\,\text{eV Å}^{-3}$, $C_{44} = 0.761\,\text{eV Å}^{-3}$, and the cohesive energy of 4.316 eV.

We choose to parametrize the potential using a polynomial spline functional form. This choice is arbitrary, but does not constrain the physical behaviour—we have shown [29] that a liquid simulation using a cubic spline fit can be used to fit a reciprocal power series potential, and the resulting $V(r)$ and $\phi(r)$ are indistinguishable.

Thus

$$\phi(r_{ij}) = \sum_k A_k (R_k - r)^3 H(R_k - r) \tag{2}$$

$$F(x) = -\sqrt{x} + a_2 x^2 + a_4 x^4. \tag{3}$$

For the extreme short range repulsion, which is sampled only by the primary knock-on atom in a cascade simulation and not by any of our fitting data, we adopt the screened electrostatic form of Biersack and Ziegler [30]:

$$V(r) = \sum_k a_k (r - r_k)^{n_k} H(r_k - r) H(r - r_2) + H(r_2 - r) H(r - r_1) \exp(B_0 + B_1 r + B_2 r^2 + B_3 r^3) + H(r_1 - r) \frac{Q_i Q_j}{r} \xi(r/r_s) \quad (4)$$

where Q_i and Q_j are the nuclear charges and where $r_s = 0.468\,3766/(Q_i^{2/3} + Q_j^{2/3})$;

$$\xi(x) = 0.1818 e^{-3.2x} + 0.5099 e^{-0.9423x} + 0.2802 e^{-0.4029x} + 0.028\,17 e^{-0.2016x}. \quad (5)$$

In these equations, $H(x)$ is the Heaviside function and r_B the Bohr radius. The B_i coefficients are determined by continuity of the potential and its derivative, and so the parameters available for fitting are A_k, a_k and C.

We take V_{FeFe}, ϕ_{FeFe} and F_{Fe} from our previous paper [13]. The ϕs are taken by scaling the pure iron values. The implicit assumption is that in the rigid band picture, the tight binding energy goes parabolically with number of valence d electrons: $(10 - N)N$. We assume that in the dilute alloy the three phosphorus valence electrons are donated to an unchanged d band. This suggests that the bond strength is e.g. $\Phi_{FeP}/\Phi_{FeFe} = (3(10-3)/6(10-6))^2 = 0.765\,625$ the squaring coming from the assumption that the embedding function is a square root. Obviously, this means that the potential is invalid for high phosphorus concentration.

To fit the remaining parameters, we use a weighted least squares fit to the lattice parameter and formation energy for several Fe_3P compounds ($D0_3$, $L1_2$, stripe), the relative energies of defect structures (including the ⟨100⟩, ⟨110⟩ and ⟨111⟩ mixed interstitial configurations), vacancy–substitutional interaction and vacancy migration energies from the first-principles calculations.

In the weighting, prime importance was placed on those configurations expected to be seen in simulation: the stable [110] interstitial, the substitutional phosphorus and the migration barriers. While other configurations were less strongly weighted, we ensured that they remained sufficiently high in energy that they would not subsequently participate spuriously in dynamics.

For the defects, as with the liquid, the fitting process is a self-consistent one—we fit to unrelaxed defect configurations to obtain a trial potential, relax the configuration using this potential, then refit the potential to the new configuration. After several iterations, a self-consistent set of defect and liquid configurations, energies and potential parameters is obtained. This process means that the interatomic distances found in the *ab initio* are not fitted. Once a fit had been obtained, the functions $V(r)$ and $\phi(r)$ were tested *ab oculo* for overfitting and MD simulations for thermal expansion, elastic moduli (figure 1), vacancy and interstitial migrations and liquid state diffusion were done as a check for pathologies. Defect properties calculated with the potential are given in table 4. The parameters for the final potential are given in table 5.

3. Phosphorus diffusion mechanisms

3.1. The interstitial mechanism of migration deduced ab initio

The models of P atom segregation proposed so far [32–34] are developed for the case when the binding energy of a phosphorus–interstitial complex is small. Specifically, the mean free path up to thermally activated dissociation is much shorter than the mean distance between sinks of

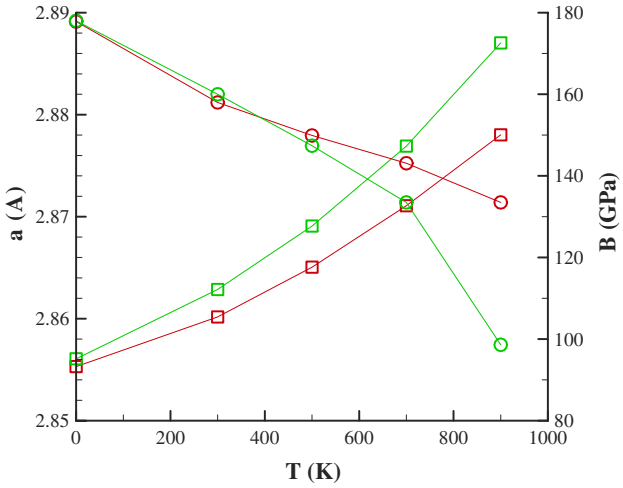

Figure 1. The effect of 10% P on the Fe lattice parameter (squares) and bulk modulus (circles), evaluated by molecular dynamics simulation on a 2000-atom $Fe_{90}P_{10}$ cell (grey (green) lines). For comparison similar quantities for pure Fe (black (red) lines) are shown.

point defects. This condition is needed to justify the detailed balance approximation, required for the concentration of P–interstitial complexes to be a function of the local concentration of P atoms. Our *ab initio* calculations show that the binding energy of a Fe–P mixed dumb-bell is not small, and hence this approximation is not valid. Indeed, the large binding energy and small migration energy of an Fe–P interstitial complex implies that during the lifetime of this complex the probability that it will dissociate thermally is small. For a typical value of phosphorus concentration in RPV steels, $\sim 10^{-3}$, the mean free path of an irradiation produced Fe–Fe dumb-bell before encountering a P atom is just a few nanometres. Hence, the majority of interstitials arriving at a GB (or any other sink of point defects) will contain phosphorus atoms. As a consequence, the phosphorus–interstitial complex should be treated as a single migrating entity in methods such as kinetic Monte Carlo simulation.

3.2. Vacancy mechanism of migration

Our results also show significant vacancy–P atom interaction energy: the binding energy of this complex is $\sim$0.3 eV. This was not expected previously and in the model by Lidiard [33] this interaction was totally neglected. Even more importantly the interaction is long ranged, at least up to the second-neighbour atoms, which invalidates the simple models [32] for diffusion coefficients of Fe–P alloy. Their conclusion, that in bcc alloys solute atoms always drift up the vacancy concentration gradient [32], must be re-examined allowing for longer ranged interactions and complex formation. The long range vacancy–phosphorus interaction in bcc iron makes it possible for a vacancy to move around the P atom, while remaining bound as a complex. As a consequence the situation may become similar to that for fcc alloys, where the diffusion coefficient of a solute atom can be positive (indicating drag of solute atoms) or negative (simple exchange) depending on the relative frequencies of vacancy jumps between two neighbour sites of the solute atom and away from the solute atom. Hence, it is possible that vacancies would drag P atoms to sinks of point defects.

The small energy for the vacancy–P atom exchange jump (relative to that of vacancy iron atom) implies that the diffusion coefficient of phosphorus atoms via a vacancy mechanism

Table 5. The analytic form of the potentials. ξ is the short range screening function [30] described in the text. As further work is done, we intend to continue the self-consistent fitting process to improve the potential. Users are encouraged to contact the authors with results and an evolving 'best' set of parameters will be maintained online at http://homepages.ed.ac.uk/graeme

Potential	Value (eV)	Cut-offs (Å)
$V_{\mathrm{FeFe}}(r)$	$9734.236\,589\,2908\xi(r, 26, 26)/r$	0.0–1.0
	$+ \exp(7.412\,270\,938\,4068 - 0.641\,806\,907\,133\,67r$	1.0–2.05
	$- 2.604\,354\,796\,1722r^2 + 0.626\,253\,939\,3123r^3)$	
	$- 27.444\,805\,994\,228(2.2 - r)^3$	2.05–2.2
	$+ 15.738\,054\,058\,489(2.3 - r)^3$	2.05–2.3
	$+ 2.207\,711\,873\,3936(2.4 - r)^3$	2.05–2.4
	$- 2.498\,979\,905\,3251(2.5 - r)^3$	2.05–2.5
	$+ 4.209\,967\,649\,4795(2.6 - r)^3$	2.05–2.6
	$- 0.773\,612\,941\,297\,13(2.7 - r)^3$	2.05–2.7
	$+ 0.806\,564\,149\,377\,89(2.8 - r)^3$	2.05–2.8
	$- 2.319\,435\,892\,4605(3.0 - r)^3$	2.05–3.0
	$+ 2.657\,740\,612\,8280(3.3 - r)^3$	2.05–3.3
	$- 1.026\,041\,693\,3564(3.7 - r)^3$	2.05–3.7
	$+ 0.350\,186\,158\,919\,57(4.2 - r)^3$	2.05–4.2
	$- 0.058\,531\,821\,042\,271(4.7 - r)^3$	2.05–4.7
	$- 0.003\,045\,882\,455\,6234(5.3 - r)^3$	2.05–5.3
$V_{\mathrm{FeP}}(r)$	$(5615.905\,724\,5908/r)\xi(r, 26, 15)$	0.0–1.0
	$+ \exp(10.761\,854\,424\,88 - 10.004\,045\,788\,895r$	1.0–2.0
	$+ 4.985\,425\,447\,2397r^2 - 1.259\,978\,856\,9372r^3)$	
	$- 3.313\,660\,574\,3629(5.3 - r)^4$	2.0–5.3
	$+ 12.625\,238\,193\,60(5.3 - r)^5$	2.0–5.3
	$- 20.361\,693\,308\,072(5.3 - r)^6$	2.0–5.3
	$+ 17.629\,292\,543\,942(5.3 - r)^7$	2.0–5.3
	$- 8.812\,072\,804\,7659(5.3 - r)^8$	2.0–5.3
	$+ 2.549\,428\,860\,9989(5.3 - r)^9$	2.0–5.3
	$- 0.396\,983\,907\,834\,03(5.3 - r)^{10}$	2.0–5.3
	$+ 0.025\,779\,015\,833\,433(5.3 - r)^{11}$	2.0–5.3
$V_{\mathrm{PP}}(r)$	$(3239.945\,610\,3409/r)\xi(r, 15, 15)$	0.0–0.9
	$+ \exp(9.938\,284\,249\,9617 - 8.563\,716\,427\,2526r$	0.9–2.5
	$+ 3.451\,962\,728\,599r^2 - 0.614\,538\,313\,502\,15r^3)$	
	$- 0.078\,293\,794\,709\,143(5.3 - r)^4$	2.5–5.3
	$+ 0.037\,557\,214\,911\,646(5.3 - r)^5$	2.5–5.3
$\phi_{\mathrm{FeFe}}(r)$	$11.686\,859\,407\,970(2.4 - r)^3$	0.0–2.4
	$- 0.014\,710\,740\,098\,83(3.2 - r)^3$	0.0–3.2
	$+ 0.471\,935\,270\,759\,43(4.2 - r)^3$	0.0–4.2
$\phi_{\mathrm{FeP}}(r)$	$\phi_{\mathrm{FeFe}}(21/24)^2$	0.0–4.2
$\phi_{\mathrm{PP}}(r)$	$\phi_{\mathrm{FeFe}}(21/24)^4$	0.0–4.2
$F_{\mathrm{Fe}}(\rho)$	$-\sqrt{\rho} - 6.731\,411\,558\,6063 \times 10^{-4}\rho^2 + 7.651\,490\,560\,4792 \times 10^{-8}\rho^4$	
$F_{\mathrm{P}}\rho$	$-\sqrt{\rho} + 0.001\,195\,027\,454\,0243\rho^2$	

would be independent of this energy. The potential shows that the barrier for jumps from first to second neighbours is similar to barriers in pure Fe. Finally, the conclusion [33] that the migration of phosphorus atoms to grain boundaries is predominantly via the interstitials has to be verified in the view of strong long ranged interaction of vacancy–P atom complexes, and

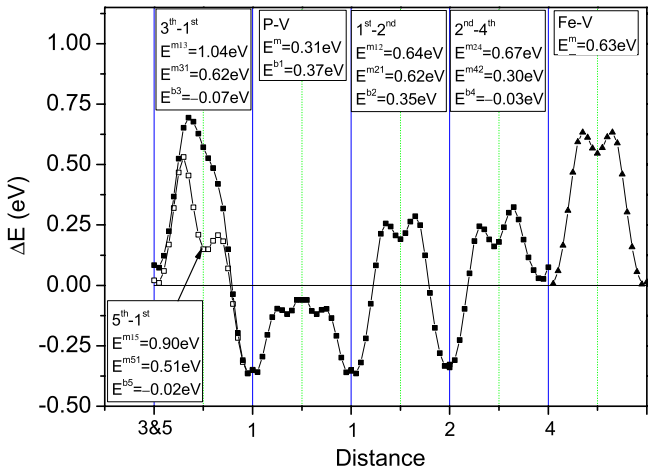

Figure 2. Constrained static relaxations of P–vacancy complexes with P moved over various barriers. E^{mxy} gives the height of the barrier to P moving from the xth neighbour to the yth; E^{bx} gives the binding energy of P at the xth-neighbour site. The final panel shows the barrier to vacancy movement in pure iron. The barrier against motion of the vacancy–phosphorus complex is similar to the binding energy, and much lower than the barrier in pure Fe. Consequently, the P traps the vacancy, reducing overall vacancy diffusion.

rates of production of single interstitials smaller than those of single vacancies in high energy displacement cascades in α-iron due to higher intra-cascade clustering of interstitial atoms.

3.3. The calculated mechanism of migration, using the potential

We have performed simulations of diffusion for point defects in FeP using the potential defined in table 5. We find that vacancies diffuse freely in iron, but are attracted to and form complexes with the P atoms. Although the phosphorus atom can move into the vacant site, in isolation this would simply produce a thermally activated oscillation, and no net diffusion—the vacancy has to hop out to second-neighbour sites and back again for comigration to occur. Using static relaxation, we calculated the various barriers to vacancy jumps in the vicinity of a P atom (figure 2). A near neighbour hop in bcc crosses two intermediate (111) planes, so the barriers tend to be bimodal. Although the P–v migration barrier is only half that of the Fe–v barrier, to obtain long range P migration the vacancy has to hop around the P via second neighbours. Energetics (both *ab initio* and with the potential) show the P to be bound to the vacancy in both first- and second-neighbour sites; however, from the second-neighbour site the barriers are similar for hopping back or further away from the P. Thus P acts as a strong vacancy trap, and comigration is likely.

We performed some preliminary MD simulations using the potential with 2000 atoms to check the mechanism and ensure against pathological behaviour. For 1200 K, with a single P interstitial, a series of 1D migration steps were observed for about 80 ps, after which the interstitial dissociated from the P atom and standard 3D migration in pure Fe continued. At 920 and 600 K, however, the mixed interstitial did not separate and migration was more three dimensional (figure 3). Interstitials diffuse freely in pure iron, and are strongly attracted to substitutional P. The P–Fe mixed dumb-bell is also highly mobile, and the P diffuses rapidly. Thus P diffusion occurs primarily via interstitials in radiation damage conditions where Fe–Fe interstitials are commonplace. Under thermal conditions however, interstitial mediated

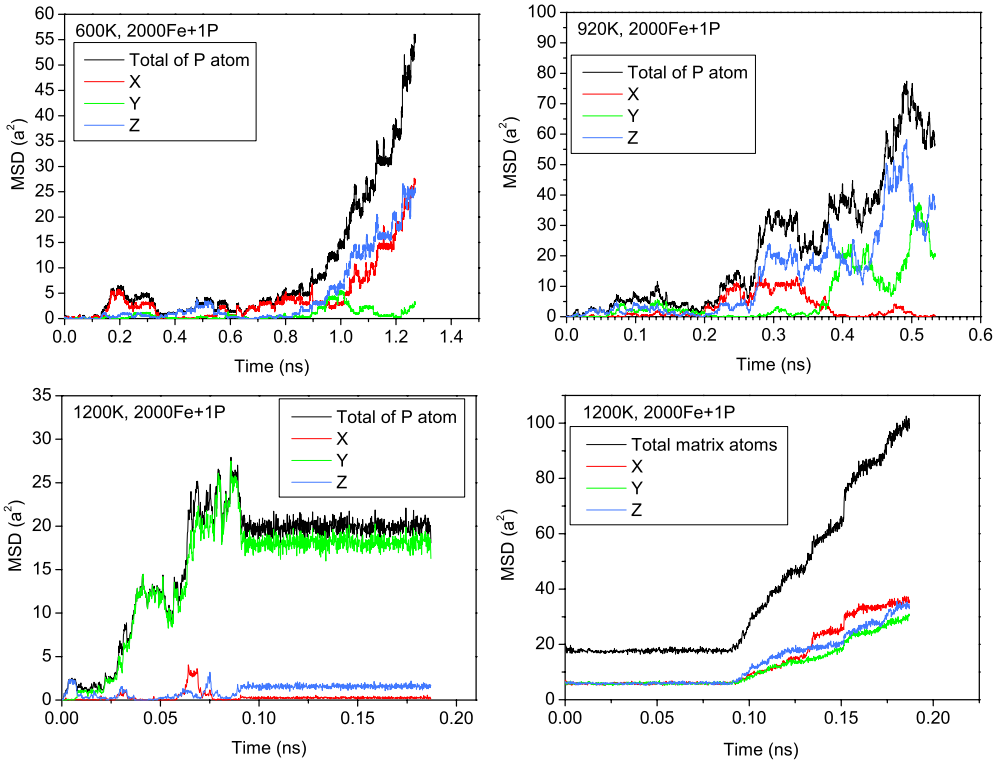

Figure 3. Mean squared displacement (MSD) against time for migration in a unit cell containing 1 P and 2000 Fe atoms, initially located in a mixed dumb-bell. Various temperatures were examined. At 600 and 920 K the P remains attached to the interstitial throughout the period of the run. For 1200 K, we observed rapid 1D diffusion of the phosphorus atom via mixed interstitial (Fe does not diffuse in this phase), followed by a dissociation event and standard interstitial diffusion in pure Fe. The simulation box is large enough that the interstitial is not recaptured, and subsequent diffusion is for the iron atoms.

segregation to boundaries will not occur since there is no source for interstitials in the bulk, and mixed interstitials formed at sinks cannot transport further P atoms to the sink.

The stability of small complexes suggests, however, that still larger complexes may be important. For example mixed interstitials may be pinned by other P atoms, forming sessile PP interstitials. Future molecular dynamics simulation can incorporate features neglected by this model, such as clustering, recombination, segregation and the specific defect distributions associated with thermal, electron or neutron radiation.

4. Conclusions

We have developed an interatomic potential for the α-Fe–P system in the limit of low P concentration with particular importance attached to configurations observed under radiation damage. This potential gives a good description of point defect properties and conformations, in particular vacancy and interstitial complexes with a P atom, and hence can be used in larger scale molecular dynamics or Monte Carlo simulations to study diffusion properties and segregation of P under both ageing and irradiation conditions. Pure phosphorus cannot be described by this type of potential.

The potential predicts that phosphorus is strongly bound to both vacancy and interstitial defects, in accordance with *ab initio* results. This had not been expected previously, and conclusions of theoretical studies that ignore strong P–defect binding should be re-examined.

We have presented preliminary molecular dynamics studies of P diffusion in iron which show the potential to be free from pathologies, but a quantitative study of these processes (which should include larger complexes) in beyond the scope of this paper. It appears that in the temperature region of interest for RPV steels P would migrate rapidly via both interstitial and vacancy complex mechanisms, although we have not studied large complexes which may further complicate the process.

In summary, the detailed understanding of radiation damage in steels remains an area of active interest more than thirty years after the pioneering work of Michael Norgett helped pose the questions.

Acknowledgments

AVB acknowledges financial support from the European Commission via contract FIKS-CT-2000-00080 ('PISA'), GJA from framework 6 project PERFECT.

References

[1] Nishiyama Y, Bloomer T E and Kameda J 2000 *Microstructural Processes in Irradiated Materials* ed G E Lucas, L L Snead, M A Kirk Jr and R G Elliman (Pittsburgh, PA: Materials Research Society) p R6.10
[2] Buswell J T, Bolton C J, Wooton M R, Bischler P E J, Jones R B, Jones L T, Phythian W J and Sinclair R 1993 *Effects of Radiation on Materials* (*ASTM STP* vol 1175) p 332
[3] Norgett M J and Fletcher R 1970 *J. Phys. C: Solid State Phys.* **3** L190
[4] Norgett M J 1970 *The DEVIL Program* unpublished
see also Thetford R 1985 *Harwell Report* AERE-M.3507 HMSO, London
[5] Norgett M J, Perrin R C and Savino E J 1972 *J. Phys. F: Met. Phys.* **2** L73
[6] Bristowe P G, Crocker A G and Norgett M J 1974 *J. Phys. F: Met. Phys.* **4** 1859
[7] Cyrot-Lackmann F 1968 *J. Phys. Chem. Solids* **29** 1235
[8] Finnis M W and Sinclair J E 1984 *Phil. Mag.* A **50** 45
[9] Ackland G J, Finnis M W and Vitek V 1988 *J. Phys. F: Met. Phys.* **18** L153
[10] Ackland G J, Bacon D J, Calder A F and Harry T 1997 *Phil. Mag.* A **75** 713–32
[11] Ackland G J and Verdozzi C 1999 *Temporal Embedding* (*MRS Symp. Proc.* vol D3)
see also Ackland G J 2002 *J. Phys.: Condens. Matter* **14** 2975
[12] Han S, Zepeda-Ruiz L A, Ackland G J, Car R and Srolovitz D J 2002 Self-interstitials in V and Mo *Phys. Rev.* B **66** 220101
[13] Mendelev M I, Han S W, Srolovitz D J, Ackland G J, Sun D Y and Asta M 2003 *Phil. Mag.* A **83** 3977
[14] Ackland G J, Tichy G I, Vitek V and Finnis M W 1987 *Phil. Mag.* A **56** 735
[15] Lopasso E M, Caro M, Caro A and Turchi P E A 2003 *Phys. Rev.* B **68** 214205
[16] Kohn W and Sham L J 1965 *Phys. Rev.* **140** 1133A
[17] Vanderbilt D 1990 *Phys. Rev.* B **41** 7892
[18] Perdew J P, Chevary J A, Vosko S H, Jackson K A, Pederson M R, Singh D J and Fiolhais C 1992 *Phys. Rev.* B **46** 6671
[19] Domain C and Becquart C S 2002 *Phys. Rev.* B **65** 024103
[20] Han S W, Zepeda-Ruiz L A, Ackland G J, Car R and Srolovitz D J 2003 *J. Appl. Phys.* **93** 3328
[21] Wu R, Freeman A L and Olson G B 1992 *J. Mater. Res.* **7** 2403
Freeman A L and Olson G B 1994 *Science* **265** 376
[22] Tang S, Freeman A L and Olson G B 1993 *Phys. Rev.* B **47** 2441
[23] Zhong L, Wu R Q and Freeman A L 1997 *Phys. Rev.* B **55** 11133
[24] Sagert L P, Olsen G B and Ellis D E 1998 *Phil. Mag.* B **77** 871
[25] Biedermann A, Schmid M, Reichl B M and Varga Fresnius P 1995 competitive segregation of Si and P on Fe (100) *J. Anal. Chem.* **353** 259

[26] Chambron W, Verdone J and Moser P 1975 *Fundamental Aspects of Radiation Damage in Metals: USERDA Report CONF751006* ed M T Robinson and F W Young (Washington, DC: USERDA) p 261
[27] Ackland G J and Thetford R 1987 *Phil. Mag.* A **56** 15
[28] Fujiwara T and Ishii Y 1980 *J. Phys. F: Met. Phys.* **10** 901–11
[29] Mendelev M I and Srolovitz D J 2002 *Phys. Rev.* B **66** 014205
[30] Biersack J P and Ziegler J F 1982 *Nucl. Instrum. Methods* **141** 93
[31] Ercolessi F and Adams J B 1994 *Europhys. Lett.* **26** 583
[32] Barbu A and Lidiard A B 1996 *Phil. Mag.* A **74** 709
[33] Lidiard A B 1999 *Phil. Mag.* A **79** 1493
[34] Barashev A V 2002 *Phil. Mag. Lett.* **82** 323
[35] Schober H R and Ingle K W 1980 *J. Phys. F: Met. Phys.* **10** 575